a reprint from Applied Optics

Glory of clouds in the near infrared

James D. Spinhirne and Teruyuki Nakajima

Spectrally resolved visible and infrared images of marine stratus clouds were acquired from the NASA ER-2 high-altitude aircraft during the 1987 First International Cloud Climatology Program Regional Experiment. The images were obtained by cross-track scanning radiometers. Data images at near-infrared wavelengths show frequent and readily apparent brightness features that are due to glory single scattering. The observations and subsequent analysis by radiative transfer calculations show that the glory is a significant feature of near-infrared solar reflectance from water clouds. Glory observations and calculations based on in-cloud microphysics measurements agree well. The most dramatic difference from the visible glory is that the scattering angles are significantly larger in the near infrared. The glory is also apparently more distinct in the near infrared than in the visible, as scattering size parameters are in a range that effectively produces a glory feature, and also there is less obscuration by multiple-scattering reflectance because of absorption of radiation by droplets in the near infrared. For both the visible and the near infrared, the principal factors that wash out the glory are dispersion and, to a lesser degree, the effective radius of the cloud droplet-size distribution. The obscuration by multiple scattering in optically thick clouds is secondary. Rather than being a novelty, glory observations would be an accurate and unambiguous technique to sense the droplet size of water clouds remotely.

1. Introduction

The angular distribution of radiation reflected from optically thick clouds is generally featureless. The exceptions are phenomena that result from the single-scattering component of reflectance such as cloud bows or glory. The large multiple-scattering component of reflected radiation for optically thick clouds obscures the single-scattering features, but they are nonetheless often observed. The glory in particular is well known to aircraft passengers as a bright colored circle surrounding the antisolar, or shadow, location. The glory is phenomenon that results from scattering by spherical particles.[1] The pattern of glory reflectance is known to show a dependence on the wavelength and the size distribution of the scattering particles. Observations of the glory are well known at visible wavelengths but not in the near infrared. Our topic here is a description of unique measurements of the near-infrared glory. The characteristics of the glory at near-infrared wavelengths are found to be different from those observed in the visible.

Extensive observations of the spectral reflectance of water clouds were acquired during the First International Satellite Cloud Climatology Program Regional Experiment (FIRE) of June and July 1987. The data were acquired by means of aircraft-mounted cross-track scanning radiometers. Much of the radiance data revealed persistent and readily apparent single-scattering features. The outstanding aspect of the initial data displays[2] was the much higher frequency and distinctness of the glory at near-infrared wavelengths than in the visible. The question is raised as to why that would be the case. What is different about the glory in the near infrared than in the visible? In this paper we compare the observations of the glory with calculated reflectance patterns that are based on *in situ* cloud particle measurements. The results have implications for the interpretation of cloud radiation measurements. We present an analysis of the glory at near-infrared and visible wavelengths and discuss possible applications for cloud remote sensing.

2. Experimental

Multispectral cloud reflectivity observations were obtained by two imaging radiometers flown on board the NASA ER-2 high-altitude aircraft. The observations were acquired on 11 visible channels, three

J. D. Spinhirne is with the Laboratory for Atmospheres, Code 917, NASA Goddard Space Flight Center, Greenbelt, Maryland 20771. T. Nakajima is with the Center for Climate System Research, University of Tokyo, 4-6-1 Komaba, Meguro-ku, Tokyo 153, Japan.

Received 1 September 1993; revised manuscript received 9 February 1994.

0003-6935/94/214652-11$06.00/0.

infrared window channels, and four near-infrared channels. One radiometer was the multispectral cloud radiometer, which has been described by Curran *et al.*[3] The second radiometer was a commercial Daedalus scanning radiometer, which is similar in design and function to the multispectral cloud radiometer. The instruments employ rotating scan mirrors inclined at an angle of 45° to build up radiometrically accurate data along a scan line that is perpendicular to the aircraft flight track. Data are acquired to ±42° from the zenith with approximately 5-mrad pixel resolution. By combining scan lines, images are built up from the data in a raster scan manner along the aircraft track. The nominal 19.5-km flight altitude of the ER-2 permits an approximately 38-km-wide area to be imaged at the surface. The specific wavelengths and bandwidths for observations and additional details on the radiometer instruments may be found in a previous paper.[4]

In addition to carrying the scanner radiometers, the ER-2 carried several other instruments during the FIRE field missions. A lidar system measured the variation in cloud height and cloud-top structure.[4] Also, broadband and spectral downward and upward flux measurements were obtained with stationary and rotating flux radiometers. An important experimental consideration is the calibration of the imaging radiometer data. Although the thermal channels are internally calibrated from two blackbody targets, which are viewed on the upward part of the scan mirror's rotation, the visible and the near-infrared channels must be calibrated from integrating-sphere standard sources before and after flight missions. Calibration accuracy is no better than 5%.

The FIRE marine stratus experiment in 1987 was designed as a comprehensive study of marine stratus clouds off the coast of southern California. The purpose of the experiment was to study meterology, cloud physics, and remote sensing related to the persistent low-level stratus clouds that form over the ocean off the California coast primarily in the spring and summer.[5] In addition to remote sensing from the ER-2, in-cloud measurements of particle and thermodynamic variables were provided by three other aircraft. A total of 10 observation days were flown by the ER-2 in the experiment. Cloud conditions for observations were mostly solid, thick stratus. As aircraft flight tracks were flown with close coordination between the ER-2 and the cloud physics aircraft, the ER-2 remote observations may be correlated with direct in-cloud particle and thermodynamic measurements.

3. Glory Observations

On 29 June 1987 the ER-2 aircraft with on-board radiometers overflew an area of mostly solid marine stratus 500 km southwest of San Diego, Calif. For a time period between 20:00Z and 22:00Z the ER-2 flew an L-shaped flight path with a 100-km line in a southward direction and an 80-km line flown east–west. At the same time the ER-2 measurements were made, the British Meterological Office C-130 cloud physics aircraft acquired measurements at different levels within the cloud deck along the identical flight path. During the entire observation period, glory features were prominent in near-infrared radiometer data.

Cross-track scanning radiometer data for the marine stratus at 3.74- and 0.74-μm wavelengths are shown in Figs. 1(a) and 1(b), respectively. In the images for both wavelengths the contrast is enhanced to make variations in radiance more apparent. As may be seen, pronounced linear brightness features are present in the 3.74-μm wavelength data. The linear features are in the direction of the aircraft flight heading. Correspondingly the features are absent from the 0.74-μm image. The image at the 2.16-μm wavelength for the same flight segment is given in Fig. 1(c). A linear brightness feature is also apparent in the 2.16-μm data but with an angular disitribution different from that of the 3.74-μm data. The data in the example are from a north–south flight line flown toward the Sun. The linear brightness features were also apparent in the data of east–west flight lines, but the pattern was offset in its angular location.

The linear brightness features may be explained by reference to Fig. 2. Single scattering would be expected to produce circular glory patterns in reflected light, which are centered around the antisolar point. Let the solar zenith and azimuth angles be θ and α, respectively, and let the aircraft be on a heading ϕ. When scanning through angle η, the radiometer will see a cross track, which is indicated by the dashed line in Fig. 2, that will intersect the circular scattering pattern as shown. There would be zero, one, or two intensity maxima, depending on whether the scan lay outside of, tangent to, or across the pattern, respectively. As the circular pattern would appear to travel along with the aircraft, the cross-track image would show linear features, as are apparent in Figs. 1(a) and 1(c).

By simple geometric considerations it is possible to relate the observed intensity pattern in the linear scans to the angular scattering pattern of single scattering that is referenced to the incident solar direction. If the cross-track scan angle from nadir is η, then from the geometry shown in Fig. 2, the single-scattering angle ψ will be given by

$$\cos\psi = \sin\eta \sin\theta \sin(\alpha - \phi) - \cos\theta \cos\eta. \quad (1)$$

The range of scattering angles that may be observed by a cross-track scan is dependent on the aircraft heading and the solar position. The 180°, or backward from the solar direction, scattering will be observed only if the aircraft heading is perpendicular to the plane that contains the Sun and the local surface normal (solar plane). Also the symmetry of the scattering pattern will depend entirely on the homogeneity of the cloud that is observed. Otherwise a different angular scattering pattern would arise at different areas in the cross-track image, producing irregularities in the observed linear bright-

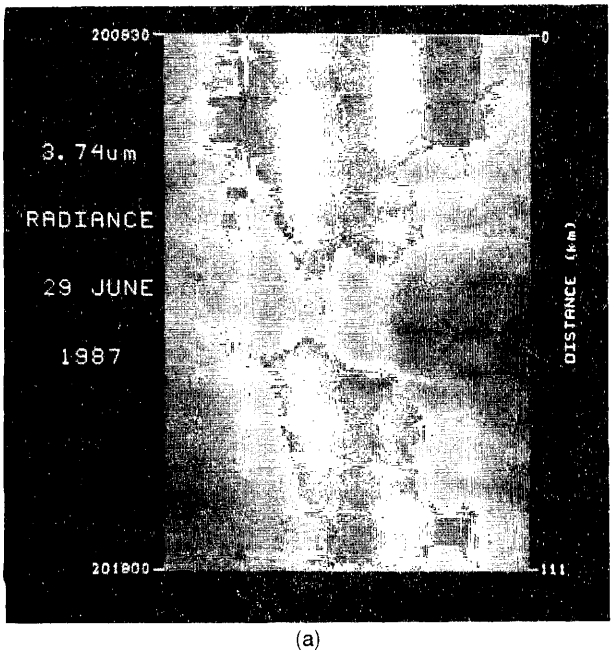

(a)

(c)

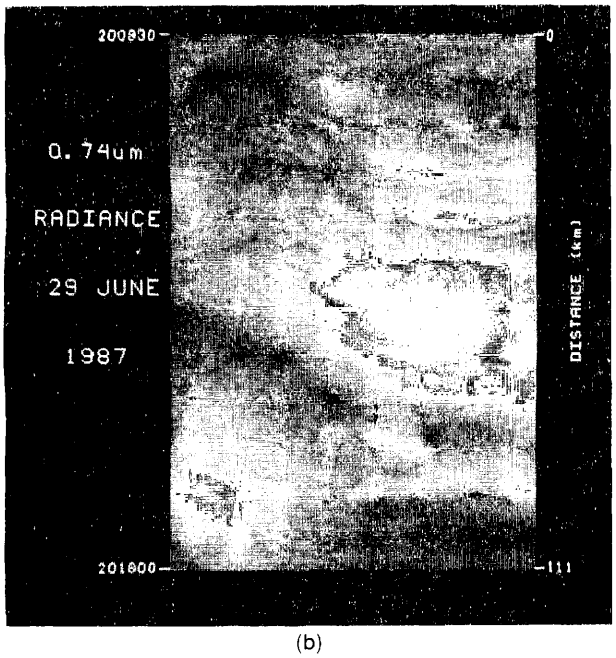

(b)

Fig. 1. Images of an area of marine stratus clouds that were obtained by visible and infrared cross-track scanning radiometers on the ER-2 high-altitude aircraft. The data were obtained on 29 June 1987 in an area southwest of San Diego, Calif. The beginning and the ending times for the images are indicated in the upper and the lower left-hand sides, respectively; distances along the flight path are indicated on the right-hand side. The area of cloud represented by the image would be approximately 36 km cross track and 114 km along the track. The along-track direction is from top to bottom in the images. The wavelengths of the images are (a) 3.74 μm, b) 0.74 μm, and c) 2.16 μm. The linear brightness features that are seen in the near-infrared images are identified here as resulting from glory single scattering. The images are presented with increased contrast in order to bring out reflectance variations. When the images were acquired the ER-2 aircraft heading was almost directly toward the solar azimuth position. The solar zenith angle at the time of the measurement was 8°.

ness features. Some variability is seen in both Figs. 1(a) and 1(c). In the middle of the aircraft flight track the linear brightness feature is less apparent. Also the angular displacement from the scan center is nonuniform. From the visible reflectance image in Fig. 1, the middle of the flight track for the data corresponds to an area where the cloud deck is brighter and thus more optically thick than other areas. Other inhomogenities are also seen.

The stratus clouds are sufficiently homogeneous along most of the cross-track scan, however, that a meaningful analysis of the angular reflectance pattern is possible. The observed radiance for the 3.74-μm wavelength as a function of the scattering angle (shown as the backscattering angle defined as $180° - \psi$) is shown in Fig. 3(a). The plot is an average of the data from the first third of Fig. 1. For the given aircraft heading and solar position, the minimum observed backscattering angle is 8°. The two curves are for the positive and the negative scattering angles separately. The radiances are shown in relative units. The effect of inhomogeneity is again seen in the difference of the two curves. There are two clearly defined peaks to the intensity distribution. The first intensity peak at approximately 13° backscattering angle is the glory peak. The smaller maxima at approximately 29° is possibly analogous to the visible-wavelength rainbow peak. The corresponding scattering plot for the 2.16-μm wavelength is shown in Fig. 3(b). A glory maximum

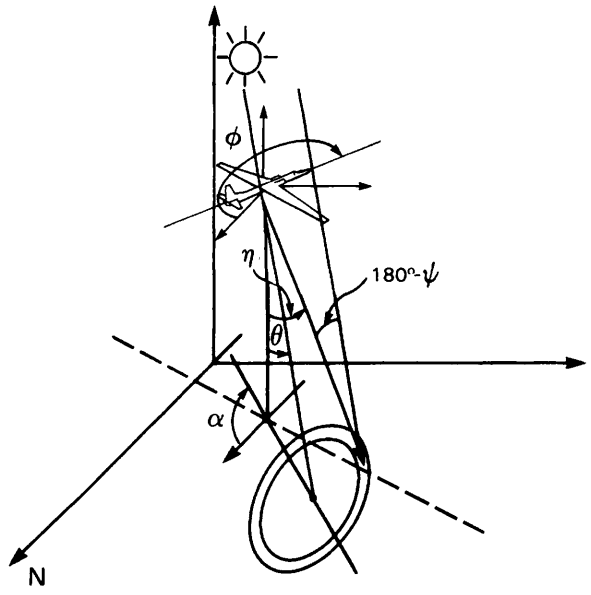

Fig. 2. Geometry for cloud scattering and the aircraft cross-track radiometer that results in the appearance of the glory scattering as linear brightness features in the radiometer images. The circular glory scattering pattern moves along with the aircraft. The dashed line represents a scan track of the radiometer, and η is the scanner zenith view angle. The angle $180°$-ψ is referred to here as the backscattering angle, where ψ is the single-scattering angle of solar radiation from the cloud to the radiometer. The solar azimuth and zenith angles are designated as α and θ, respectively, and the aircraft heading as ϕ.

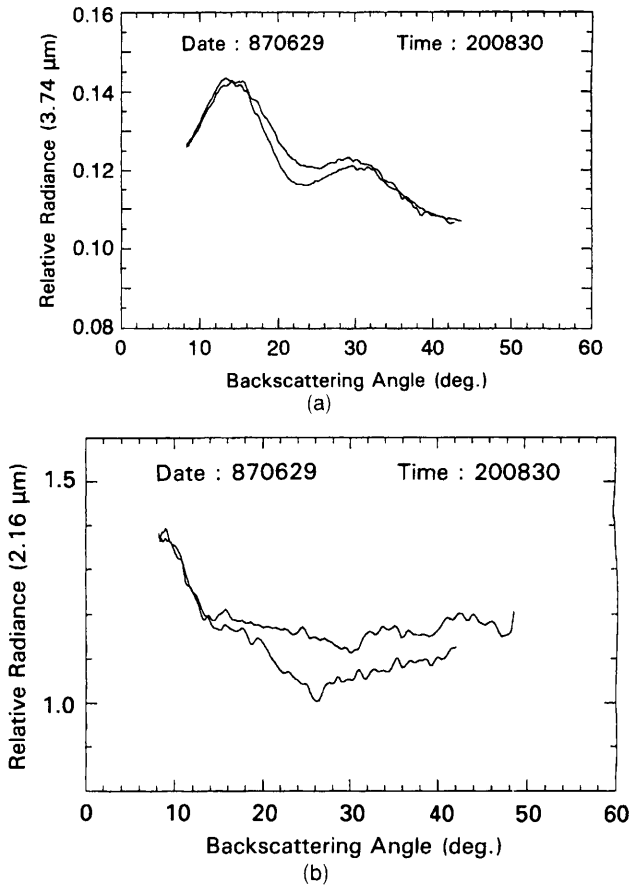

Fig. 3. Relative intensity of reflected solar radiation as a function of the solar backscattering angle $180°$-ψ for the 29 June marine stratus observations. The curves are the along-track average of the first one-third of the data shown in Fig. 1. For each wavelength the values for the positive and the negative zenith angles of the radiometer scans are shown as separate curves. The beginning of the curves at approximately 8° is the minimum observed scattering angle that results from the scans not lying in the solar plane. The difference in the two curves is a result of inhomogeneity of the cloud scene. The difference in cloud optical properties at 3.74 and 2.16 μm gives rise to a difference in the influence of the cloud inhomogeneity. Also the scattering at 3.74 μm results in a secondary single-scattering peak at ~29°. The secondary peak is not found for 2.16 μm.

of less than or equal to 8° is found. Results for the 1.64-μm wavelength (not shown) are similar to that for 2.16 μm with an intensity maxima that is at a backscattering angle that is less than the observed range of angles.

The observation of linear brightness features in near-infrared-wavelength images was not restricted to the 29 June case. For the 10 ER-2 observational days of the 1987 marine stratus experiment, the near-infrared glory maxima were easily apparent for all measurements in which the observed single-scattering angles were sufficiently small. Some of these clouds had an estimated optical thickness of greater than 30. At the initial discovery of the linear brightness features in the cross-track scanner images, we were surprised that the features were prevalent in most of the near-infrared data but were not seen in the visible-wavelength data. It is now known that the observed single-scattering angles were typically larger than the range in which the visible-wavelength glory would be observed.

It is of interest whether the glory maxima in the near infrared are much stronger than those in the visible. In one case during the 1987 marine stratus experiment, the linear brightness features were seen in the radiometer images for both the near-infrared and the visible channels. Data images from the case on 11 July 1987 as shown for the 3.74- and 0.74-μm wavelengths in Fig. 4. When the data were acquired the ER-2 was flying in a south–southeast direction in one of a series of flight lines directly over an instrumented field site located on San Nicholas Island off the southern California coast. There were no low-altitude aircraft in the region at the time to provide *in situ* microphysical measurements as a result of problems with air traffic control. In the flight line, which extends from 21:15 to 21:23Z, there is a relatively strong glory-related linear brightness features in the 3.74-μm data and a fainter one in the 0.74-μm data. There is a distinct difference in the glory pattern between the first and the last half of the data. In the last half of the images, the separation between the glory peaks is smaller, and a central intensity peak becomes evident. When the average of the cross-track scan radiance at 3.74 μm for the first and the last halfs of the image are plotted as a function of the single-scattering angle, Fig. 5, it is seen that the glory intensity maxima change from approximately 17° to

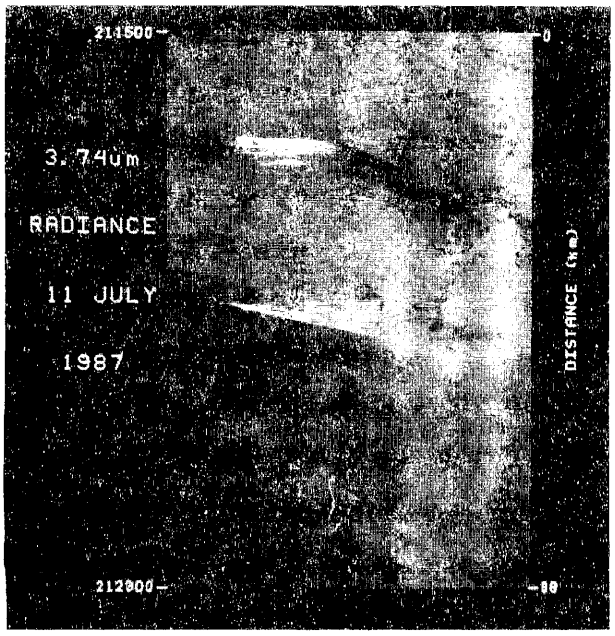

(a)

(b)

Fig. 4. Spectral images of a marine stratus cloud layer near San Nicholas Island, Calif., that were acquired on 11 July 1987. The ER-2 aircraft flight track was perpendicular to the solar plane, and the solar zenith angle was 19°. Linear brightness features from the glory are found for both the near-infrared and the visible-wavelength data. On the left-hand side of the images, sun glint can be seen through breaks in the cloud deck.

9° between the two cloud regions. As above, both the curves for the positive and the negative scattering angles in Fig. 5 are separately shown, and some variation that is related to cloud inhomogeneity is noted. For the scan average from the first half of the data an intensity peak is also seen at ~37° and is in fact not due to cloud scattering but is the result of sun glint from the ocean surface below the cloud layer.

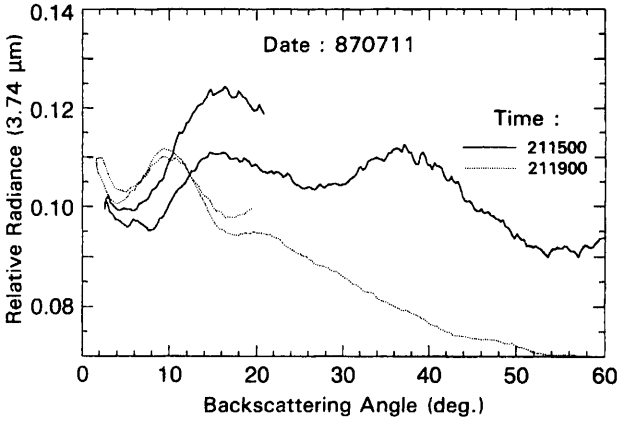

Fig. 5. 3.74-μm radiance as a function of the backscatter angle that corresponds to the Fig. 4 images. Shown separately are the along-track average of the first four and last four minutes of the data in Fig. 4. For each time period the result for the positive and the negative zenith observation angles are plotted individually.

The glint is clearly seen in the cloud gap at approximately one-fifth into the flight line of Fig. 4. The view of the surface glint plus the low overall cloud reflectance is an indication that the clouds in the first half of the images are much optically thinner than in the last half. The thinness of the cloud layer is verified by the coincident lidar data that were obtained simultaneously with the radiometer observations. For the first half of the flight line, laser returns from the surface were obtained through the cloud layer, which indicates that the visible optical thickness was less than approximately three. For the last half of the flight line, no lidar surface returns were seen.

For the data of 11 July, the aircraft flight line was nearly perpendicular to the solar plane, and the cross-track radiometer scans were cutting almost through the center of the circular single-scattering features. As seen from Fig. 5 scattering angles down to less than 2° from the backward direction were observed. A relatively strong glory pattern is evident in the visible data for the last half of the flight line. The relative intensity as a function of the backscattering angle for the average of those data is shown for two near-infrared wavelengths and the 0.74-μm wavelength in Fig. 6. The angular displacement of the glory intensity peak from the backscatter direction increases with wavelength from 1.5° at 0.74 μm to 9° at 3.74 μm. The magnitude of the glory peaks, that is, the change in intensity from the nearby cloud region to the peak, does not change appreciably from one wavelength to the other. However, the relative intensity of the peaks in relation to the average cloud brightness does change. The relative brightness of the glory peaks becomes less at the shorter wavelengths.

The general perception is that a glory is most apparent for optically thin clouds, as the background radiance that is due to multiple scattering is less. However for the 11 July case we have the situation that the glory is equally or more apparent for the

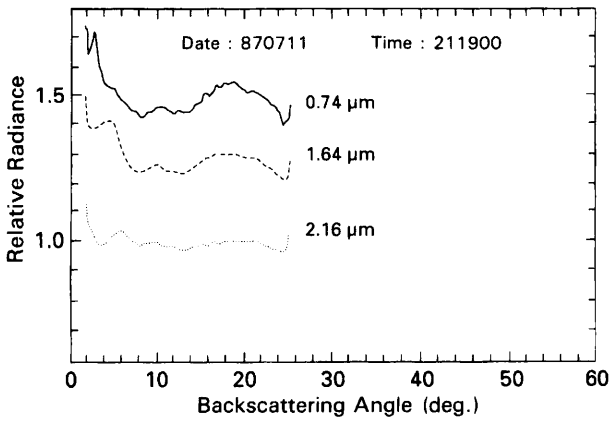

Fig. 6. As in Fig. 5 for three additional wavelengths. The curves are for the average of data from the last half of the flight line of Fig. 4. Only results from the negative portion of the zenith observation angles are shown.

optically thicker of the two different cloud regions. To explain this fact and other aspects of the observed glory features, we can gain insight from model calculations of cloud reflectance patterns.

4. Interpretation

Radiative transfer calculations of the reflectance of plane-parallel water clouds are now well known by a variety of different techniques, and general calculations of this type have been previously presented.[6] In order to analyze our observations, we performed specific calculations that simulate similar geometry and cloud layers by means of a discrete ordinate plane-parallel radiative transfer code.[7] The discrete ordinate radiative transfer code has the advantage of good computational efficiency and accuracy and gives high angular resolution.

The basis of the radiative transfer calculation is the computed single-scattering phase function for the given wavelength and the droplet-size distribution of the assumed cloud. The phase function calculation involves integration over a droplet-size distribution. In our calculations the droplet-size distribution is defined by a log-normal equation, which is given as

$$\frac{dS}{d\ln r} = \frac{1}{(2\pi\sigma)^{1/2}} \exp -\frac{1}{2}\frac{(\ln r - \ln r_2)^2}{\sigma}, \qquad (2)$$

where r is the droplet radius, and S is the cumulative cross-section density. The variable coefficient term r_2 in Eq. (2) is related to the standard[6] definition of effective mode radius r_0 by

$$r_0 = r_2 \exp(\sigma^2/2), \qquad (3)$$

where σ is the effective variance. For typical values of σ, r_0 and r_2 are nearly identically equal. The single-scattering phase function is derived from standard Mie theory calculations that are integrated over the droplet distribution. The index of refraction for water droplets is a function of wavelength, and appropriate real and imaginary values were applied in the calculations.[8] For the near-infrared wavelengths, the imaginary index leads to appreciable absorption.

As an initial comparison between the observations and the reflectivity calculations, the reflected intensity was modeled to correspond to the solar zenith angle of the data from 29 June 1987. Results are shown in Fig. 7 for the 3.74-μm wavelength for four different effective radii. The index of refraction applied in calculations is $1.374–0.0036i$, and the calculations assume a fixed liquid-water path of 0.005 g/cm^2. As the liquid-water path is held constant, the optical thickness τ for the calculations becomes a function of the mean droplet size. The calculations are for the solar plane. The results are thus equivalent to the reflectance observed by the cross-track scanning radiometers when the aircraft is in a flight line that is exactly perpendicular to the solar plane. The reflection functions are in terms of the angle from nadir rather than the angle from the solar backscatter direction. For the three larger-particle radii, the single-scattering glory component (which is centered at the solar zenith angle) is clearly evident in the calculated reflection pattern. The glory maxima for the 4-μm mode radius are present but are less distinct. The calculated angular displacement of the glory maximum changes with effective particle radius as expected. The angular displacement of the glory maximum is 12° for the 8-μm radius and 15° for the 6-μm radius.

In Fig. 7 the observed scattering angles for the 29 June glory maxima are indicated. From the comparison to the calculated values it would be expected that the effective droplet mode radius would be between 6 and 8 μm. A comparison with the droplet size measured by the British Meteorological Office C-130 aircraft[9] can be made. The mean cloud height and

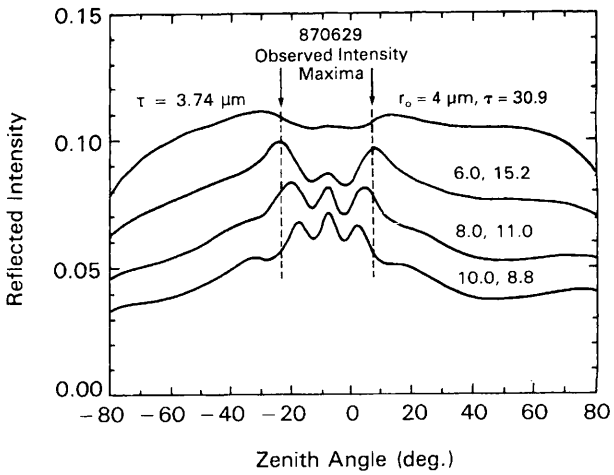

Fig. 7. Model calculation of the pattern of reflected 3.74-μm radiation from a stratus cloud shown as a function of zenith observation angles. The calculation assumes a solar zenith angle of 8° and that the observation azimuth is perpendicular to the solar plane. The vertical liquid-water path is held constant, and the optical thickness is varied as necessary for each effective droplet radius. The vertical dashed lines correspond to the positions of the maxima of the glory observed for the 29 June data in Fig. 1.

the thickness were approximately 1150 and 200 m, respectively. During the ER-2 observations the C-130 was flying at different levels in the cloud layer along the same flight track (one initial reaction when we first saw the linear brightness feature in the radiometer data was that it was contrails or cloud modification from the C-130). From the in-cloud measurement it is possible to describe the microphysics of the cloud layer. The average vertical liquid water path was 0.005 g/cm^2. The droplet size mean radius, as measured by a Forward Single Scattering Probe, changed as a function of height. Average values over the north–south flight leg are shown in Fig. 8. For the top hundred meters of the cloud layer the mean radius varied from 6 to 7 μm and decreased to approximately 4 μm at 200 m below the cloud top. The drop concentration varied from approximately 180 to 220 drops/cm.[3] By an integration based on the drop concentration, it is readily shown that 80% of the single-scattered radiation reflected from the cloud layer arose from the top 100 m of the layer. There is thus a good agreement between the measured angle of the glory maximum and the expected value based on *in situ* cloud droplet measurements. That would be expected for all cases in which measurements were good. The physics for scattering by the spherical drops is accurately described by Mie theory.

For comparison with the near-infrared glory, the glory for the visible wavelength of 0.74 μm is shown in Fig. 9 for the same cloud parameters as in Fig 7. The angular distance from the antisolar point to the glory peaks is much smaller than for the infrared. The small angles explain why the visible-wavelength glory was not seen in the cross-track scanning radiometer data for cases such as 29 June for which backscattering angles below 8° were not observed. The brightness of the visible-wavelength glory maxima, however, is not that much different than for the 3.74-μm wavelength, both for the absolute and for the relative intensity increases. The 3.74-μm radiance of clouds includes a thermal emission component that can be

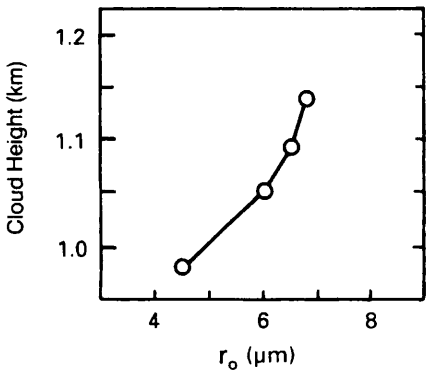

Fig. 8. Vertical profile of the effective radius of the droplet-size distributions on 29 June 1987 from in-cloud observations. The measurements are from a Forward Single Scattering Probe on the British Meteorological Office C-130 aircraft. The data points are averages along flight lines that correspond to the ER-2 track of the radiometer data in Fig. 1.

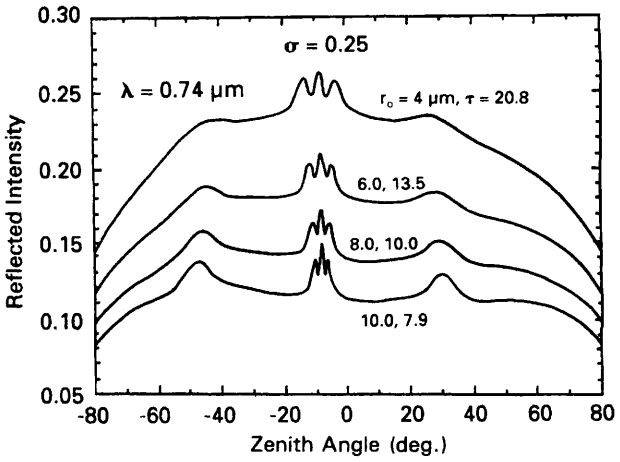

Fig. 9. As in Fig. 7 but for the 0.74-μm wavelength.

comparable in magnitude with the reflected solar component. The emission component would in general be uniform and is not included in the intensity calculation.

Several factors affect the brightness of the glory-scattering features. Optical thickness is a factor, but the absolute single-scattering radiance would not change appreciably after a cloud optical thickness has increased beyond two or three. The relative brightness of the glory will decrease as reflectance from multiple scattering increases and submerges the single-scattering reflection. However, the increase of the multiply scattered reflection of clouds asymptotically approaches a constant value. A glory maxium of 20% relative brightness at an optical thickness of 10, as shown in Fig. 7, would decrease to only approximately 10% for an infinitely thick cloud. The cloud optical thickness, for a vertically homogeneous cloud, is not the dominant factor for the visibility of the glory.

Another factor for the visibility of the glory is the effective radius and effective dispersion of the droplet-size distribution. When the scattering size parameter ($2\pi r/\lambda$) is less than approximately four, the glory peak in the scattering-phase function for spherical drops becomes negligible[6]; this is seen in Fig. 7, in which the glory is disappearing when the effective particle radius decreases to 4 μm. On the other hand, when the size parameter is in the range above approximately 150 the glory peak merges into the 180° backscatter peak. Even when the effective radius is in the range in which the glory feature is strong, however, the dispersion of the droplet distribution is important to the visibility of the glory. The effect of the dispersion of the droplet distribution is illustrated in Fig. 10. When the effective variance is increased from 0.20 to 0.35, the peak radiance of the glory maximum is decreased by half. The summed spread of angles for the glory of different particle radii decreases the brightness of the single-scattering feature. The calculation for the 3.74-μm wavelength is shown, but similar effects are found in calculations for other wavelengths.

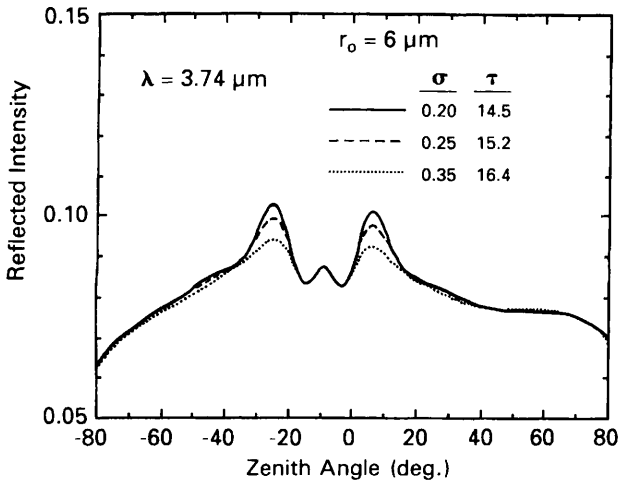

Fig. 10. Effect of the dispersion of the droplet-size distribution on the intensity of the glory pattern for the wavelength and the geometry of Fig. 1(a).

For the data of 29 June the relative variance of the droplet size distribution along a single flight level is of the order of 0.15 to 0.25 from the in-cloud measurements. An accurate vertical integration is difficult. However, if we assume that 0.25 is representative for the vertically integrated variance, the observed intensity increase for the glory feature is of the same magnitude as that calculated.

Another important effect for the glory intensity is the absorption of water as a function of wavelength. If the imaginary index of refraction is sufficiently large that there is essentially no transmission of radiation into the drop, such as wavelengths near 3.1 μm,[6] there will be no glory for scattering at any particle size. For the wavelengths applied in this paper, water attenuation is not that extreme. For the 3.74-μm wavelength the single-scattering albedo varies from 0.97 to 0.8 as the drop radius changes from 3 to 24 μm, and the glory in the scattering-phase function is still quite distinct. Another effect of water attenuation on the visibility of the glory, however, is the suppression of the background cloud brightness from multiple scattering. Water droplet clouds are generally less reflective in the near infrared than in the visible as a result of absorption effects.[10] Because of the decrease of the single-scattering albedo for larger drops, the trend is for the near-infrared reflection to decrease relative to the visible as the effective particle radius becomes larger. This is a factor for the relative brightness of the glory features.

The change in the glory angular distribution and relative brightness as a function of the cloud droplet characteristics is illustrated by the 11 July case in Figs. 4. In the first half of the image the peak of the 3.74-μm glory maximum is at an angle of 17°, which would correspond to an effective particle radius of 5 μm. For the cloud layer in the last half of the data image, the values are 10° and 10 μm, respectively. The 0.74-μm glory data give 4.2° and 4.5 μm and 2.5° and 9 μm for the same cases, or a slightly smaller effective radius from the glory. The small difference in the size interpretation could possibly be due to a different effective vertical integration of single-scattering intensity for the two wavelengths. From the visible image we know that the cloud in the last half of the flight is optically thicker than in the first half. For the 3.74-μm data the optically thicker cloud in the last half of the image is paradoxically of lower reflectivity than the adjacent optically thin cloud. The explanation is the increase in the droplet size. As mentioned above, the single-scattering albedo of water drops at 3.74 μm decreases with increasing drop size and thus the optically thicker cloud is darker at 3.74 μm because of larger droplet sizes. A similar explanation can be applied to data from 29 June, as shown in Fig. 1. In the middle of the visible image there is a bright cloud area that is darker in the near infrared.

The relative and the absolute brightnesses of the glory features for the 11 July case are generally consistent with the calculations presented above. The decrease in the absolute brightness of the glory features at 3.74 μm for the optically thick cloud in the last half of the flight line, as is most clearly seen in Fig. 5, would be best explained by a change in the dispersion of the droplet-size distributions, although there are no confirming measurements. The increase in brightness at the 3.74-μm glory maxima is approximately two times greater for the thin cloud area as for the thick cloud area. A similar effect is found for the 0.74-μm data. The brightness of the 0.74-μm glory, as shown by the image of Fig. 4(b), is deceptive. The images are presented with a compressed and offset gray scale to bring out most clearly the range of intensity in the image. The offset has the effect of eliminating areas of lowest reflectivity, and thus the glory for the first half of the flight line is only barely visible. An analysis of the data shows that the glory at 0.74 μm is in fact less intense for the last half of the flight line. The relative brightness drops from approximately 12% to 7%, which is consistent with a larger dispersion of the effective droplet-size distribution for the optically thicker cloud.

If the dispersion of the cloud droplet-size distribution is a major factor for the visibility of the glory, it might be expected that the optical bandwidth of the observation channel is a factor also. The measurements that have been presented were acquired with narrow-bandwidth channels. The 0.38-μm bandwidth of the 3.74-μm channel was the largest for our measurements. Over the wavelength bandwidth the backscattering angle of the glory would not change more than approximately 1°. As 1° is small compared with the angular width of the maxima, the bandwidth would not significantly decrease the magnitude of the maxima. For a much broader spectral bandwidth this would not be the case.

A related topic to the discussion above is the connection between narrow optical bandwidth observations of the glory and the visual visibility of the glory. Black-and-white photographs of the cloud

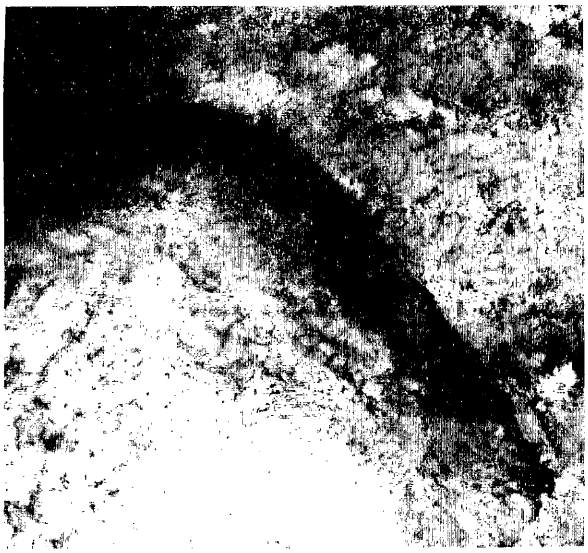

Fig. 11. Black-and-white photograph of cloud glory made from the ER-2. The picture corresponds to the data of Fig. 4. The central cloud gap seen here is at approximately a quarter of the distance down from the top of Fig. 4. Camera images were acquired for all the ER-2 flights, but this is only one of a few frames that captured a glory feature. The glory could not be seen in the pictures of the thicker clouds that directly followed this image.

tops, acquired from the ER-2, are a source for comparison. Generally the glory could not be seen in the camera images. The camera field of view, 78° for the photographs, was similar to the cross-track scan width of the radiometer data. In almost no cases in which the near-infrared glory was observed could a glory feature be seen in the camera frames. Figure 11 is one of the few camera pictures with a visible glory feature. It is from the data case of July 11, previously presented in Fig. 4. The picture is at the location of the cloud gap between the thin and the thick areas of cloud cover. Only in photos of the optically thin region, such as Fig. 11, could the glory be seen. Although the narrow bandwidth 0.74-μm data in Fig. 4(b) show a distinct glory for the optically thick cloud region, the camera images of the same region did not show a glory. The factors that obscure the visibility of the glory for broadband scenes of bright, optically thick clouds do not seem to be well related to our narrow-bandwidth observations. Quite likely image saturation, or lack of contrast perception, is a major factor. Visual observations are inherently broadband, but colors are perceived. Possibly direct visible observations or color photographs would detect cloud glory more effectively than black-and-white photography, but the question goes beyond our current investigation.

5. Discussion

For the aircraft radiometer image data, our observations and analysis indicate that the principal reason that glory features were more apparent in near-infrared wavelengths than in visible wavelengths was the larger backscattering angle involved for the near-infrared data. In addition, for the cases we have studied, the near-infrared glory is somewhat brighter in relation to the overall multiply scattered cloud reflectance than is the visible-wavelength glory. The principal factor for washing out the glory feature for water cloud reflectance seems to be the dispersion of the droplet-size distribution. The dispersion influence is possibly greater for visible than for near-infrared wavelengths, but additional analysis would be required for verying this. In general the glory should be discernible with proper observations for almost all water clouds in both visible and near-infrared wavelengths.

Measurements of the scattering angles of the glory brightness maxima could be an accurate technique for determining the effective radius of cloud top droplets. Figure 12 illustrates the direct and unambiguous relation between droplet radius and the glory angle. Curves for several wavelengths are shown, but only a measurement at a single wavelength is required for determining droplet size. From the discussion above there is also a possibility that the dispersion of the size distribution could be inferred from the brightness of the glory features. Additionally, the glory reflection results from the droplet size in a localized cloud top region. For single scattering, typically ~85% or more of the radiance arises from the first single optical thickness of the cloud top. As droplet size changes as a function of depth into the cloud, a measurement localized near the cloud top can be more readily interpreted than one that responds to the integrated cloud optics.

Remote sensing of cloud particle size is important for a number of reasons. For example there is much current interest in the Twomey effect,[11] which is the increase in reflected radiation from clouds that is due to larger numbers of smaller droplets that result from the presence of pollutants. There is also interest in other possible anthropogenic effects on cloud radiation.[12] A widely discussed remote sensing method for determining cloud droplet size uses the relation of reflectance between visible and near-infrared channels.[10] Problems with the technique include cloud geometry effects, vertical cloud inhomogeneity and

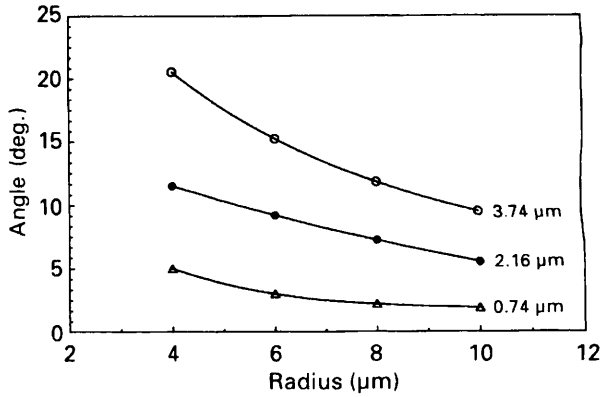

Fig. 12. Variation of the backscattering angle calculated for the glory diffraction peak as a function of the effective radius of a cloud droplet-size distribution for three wavelengths.

multiple-scattering photon penetration, instrument calibration, and the so-called anomalous absorption, which has been proposed to explain that lack of agreement between theory and measurement for the reflectance ratios.[10,13,14] By contrast, a glory angle measurement is unambiguous, and calibration is not an issue. The method does not depend strongly on liquid-water light absorption, which gives rise to the major problem of the reflection technique. Cloud inhomogeneity need not be a factor. The disadvantage is that area coverage would be limited because observations can be made only near the antisolar direction.

The use of cross-track scanner measurements, as reported here, is not an ideal way to observe single-scattering features from clouds such as the glory. Fundamentally the measurement relies on the homogeneity of the cloud scene. One of the most impressive aspects of the observations presented here is the constancy of the scanned glory pattern over significant changes of the stratus cloud structure. The patterns may have been expected to be less stable.

The best way to apply the glory scattering to droplet-size retrievals would be to measure the reflectance of individual cloud parcels from multiple view angles. This could be easily applied with modern imaging technology. The approach would be to acquire, in the antisolar direction, multiple-camera-type images of a cloud scene from a moving platform. The instrument could be as simple as a filtered CCD array camera with a PC, frame grabber and image edge analysis software for data analysis, but it is easy to conceive of more sophisticated instruments. One example of an application would be to study the variation of droplet size at cloud edges for inhomogeneneous and broken clouds. Another application would be to validate other cloud droplet-size measurements, both *in situ* and by remote sensing.

Our observations of the glory for water clouds also indicates the importance of accounting for the single-scattering features in analysis of the reflected radiation, especially in the near infrared. The near-infrared glory features will be present for a much larger range of scattering angles than in the visible. For analysis of near infrared satellite radiometer data, such as the advanced very-high-resolution radiometer 3.7-μm channel, the glory could be a significant factor for applications in which the single-scattering angle is greater than 155°. Radiative transfer codes applied for interpretation of reflected cloud radiation should have sufficient accuracy and resolution that single-scattering features are preserved.

5. Conclusions

Cloud glory is found in the scattering of solar radiation at near-infrared wavelengths just as it is for visible wavelengths. Measurement and analysis of the glory at multiple wavelengths indicate that the glory in the near infrared would be typically more prominent than for visible wavelengths. The factors that give rise to the prominence of the near-infrared glory for clouds are scattering size parameters that are effective for glory in single scattering, the somewhat suppressed multiple-scattering reflectivity of water clouds in the near infrared that is due to absorption, and the greater scattering angles of the near-infrared glory. The most dramatic difference between a visible and a near-infrared glory is the much larger scattering angles from the backward solar direction that are found for the near infrared. For the 3.7-μm wavelength, angles range from 10° to 22°, whereas the corresponding angles are less than 5° for visible wavelengths.

For both visible and near-infrared wavelengths, the overall optical cloud thickness is not the dominant factor for the visibility, or relative brightness, of the glory. Although the increase in the overall cloud reflectance from the greater multiple scattering of optically thicker clouds is a factor in reducing the relative visibility of the glory, it does not wash out the feature. Rather, the disappearance of glory features from water clouds is found to be more related to the effective radius and dispersion of the droplet-size distribution. Ratios of wavelength to particle radius at large and small extremes are less effective for glory scattering. Also, scattering from broad particle-size distributions result in glory features at a range of angles that averages out. More analysis is needed, but it is likely that these factors are less effective in obscuring the near-infrared than the visible glory. We do not find that our spectrally narrow observations are well related to the visibility of the glory for spectrally broad observations, such as black-and-white photography.

Observations of the glory in either near-infrared or visible wavelengths have good potential as an approach to measuring cloud-top droplet size through remote sensing. There is a direct dependence of the glory-scattering angle on particle size. The important and relevant characteristic is that the measurement would be unquestionably accurate and unambiguous. In this paper we have compared glory-scattering observations with simultaneous in-cloud measurements of the droplet-size distributions and have found good agreement between the two measurements. If the agreement had not been good we could only conclude that the *in situ* droplet-size measurements were in error.

Considerably more near-infrared glory observations were acquired in the 1987 marine stratus experiment than are reported here. The data, along with coincident cloud microphysics and other measurements, are now part of the generally available data archive from the 1987 experiment. One may readily conceive of additional interesting analyses and applications of the measurements for radiation and remote sensing problems.

We thank Thomas Arnold for his assistance in the processing of the data from the imaging radiometers. We also must acknowledge to the support of the NASA Ames ER-2 program and in particular the sensor group under Jeffrey Meyers. We are espe-

cially grateful for the *in situ* microphysics measurements that were provided by the late Steve Nicholls of the British Meteorological Office. This work is supported by the Radiation Science Program of the NASA Office of Physical Climate Research.

References

1. V. Khare and H. M. Nussenzveig, "Theory of the glory," Phys. Rev. Lett. **38,** 1279–1282 (1977).
2. J. D. Spinhirne and T. Nakajima, "Observation and analysis for the bi-directional reflectance of stratus clouds at near-infrared wavelengths," in *Preprint Volume of the Symposium on the Role of Clouds in Climate* (American Meteorological Society, Boston, Mass., 1989), p. 296.
3. R. S. Curran, H. L. Kyle, L. R. Blaine, J. Smith, and T. D. Clem, "Multichannel scanning radiometer for remote sensing of cloud physical parameters," Rev. Sci. Instrum. **52,** 1546–1555 (1981).
4. J. D. Spinhirne and W. D. Hart, "Cirrus structure and radiative parameters from airborne lidar and spectral radiometer observations," Mon. Weather Rev. **118,** 2329–2343 (1990).
5. B. A. Albrecht, D. A. Randall, and S. Nicholls, "Observations of marine stratocumulus clouds during FIRE," Bull. Am. Meteorol. Soc. **69,** 618–626 (1988).
6. J. E. Hansen, "Multiple scattering of polarized light in planetary atmospheres. Part II. Sunlight reflected by terrestrial water clouds," J. Atmos. Sci. **28,** 1400–1426 (1971).
7. T. Nakajima and M. Tanaka, "Algorithms for radiative intensity calculations in moderately thick atmospheres using a truncation approximation," J. Quant. Spectrosc. Radiat. Transfer, **40,** 51–69 (1988).
8. G. M. Hale and M. R. Querry, "Optical constants of water in the 200-nm to 200-μm wavelength region," Appl. Opt. **12,** 555–563 (1973).
9. S. Nicholls, "The dynamics of stratocumulus: aircraft observations and comparisons with a mixed layer model," Q. J. R. Meteorol. Soc. **110,** 783–820 (1982).
10. T. Nakajima, M. D. King, J. D. Spinhirne, and L. F. Radke, "Determination of the optical thickness and effective particle radius of clouds from reflected solar radiation measurements. Part II: marine stratocumulus observations," J. Atmos. Sci. **48,** 728–750 (1991).
11. S. Twomey, "The influence of pollution on the shortwave albedo of clouds," J. Atmos. Sci. **34,** 1149–1152 (1977).
12. L. F. Radke, J. A. Coakley, Jr., and M. D. King, "Direct and remote sensing observations of the effects of ships on clouds," Science **246,** 1146–1149 (1989).
13. F. Rawlins and J. S. Foot, "Remotely sensed measurements of stratocumulus properties during FIRE using the C130 aircraft multichannel radiometer," J. Atmos. Sci. **47,** 2488–2503 (1990).
14. G. L. Stephens and C. M. R. Platt, "Aircraft observations of the radiative and microphysical properties of stratocumulus and cumulus cloud fields," J. Climate Appl. Meteorol. **26,** 1243–1269 (1987).